

# **A 15 Simulating strongly correlated quantum systems: the density-matrix renormalization group**

Ulrich Schollwöck

Institute for Theoretical Physics C

RWTH Aachen, 52056 Aachen, Germany

## **Contents**

|          |  |           |
|----------|--|-----------|
| <b>1</b> | <b>Introduction</b>                              | <b>2</b>  |
| <b>2</b> | <b>Density-matrix renormalization group</b>      | <b>2</b>  |
| 2.1      | Decimation of state spaces . . . . .             | 3         |
| 2.2      | Finite-system DMRG procedures . . . . .          | 5         |
| 2.3      | When and why does DMRG work? . . . . .           | 9         |
| <b>3</b> | <b>Time-dependence in quantum systems</b>        | <b>10</b> |
| <b>4</b> | <b>Early attempts in DMRG</b>                    | <b>11</b> |
| <b>5</b> | <b>Adaptive time-dependent DMRG</b>              | <b>12</b> |
| <b>6</b> | <b>Error analysis: magnetization dynamics</b>    | <b>14</b> |
| <b>7</b> | <b>Spin-charge separation in ultracold atoms</b> | <b>17</b> |
| <b>8</b> | <b>Finite temperature</b>                        | <b>21</b> |
| <b>9</b> | <b>Conclusion</b>                                | <b>22</b> |

# 1 Introduction

The physics of strongly correlated quantum systems continues to pose major challenges in experimental and theoretical physics, ranging from phenomena such as Kondo physics, Luttinger liquid physics, spin chains and ladders through frustrated quantum magnets and high- $T_c$  superconductivity to bulk materials with strong correlations such as transition metal and rare earth compounds. In this context, the so-called *density-matrix renormalization group (DMRG)* [1, 2] has emerged as the most powerful method for one-dimensional strongly correlated systems. This lecture is concerned with outlining the basics of this method – for a more detailed discussion and also a complete overview over all its many fields of application, I refer to [3].

Among these applications, one stands out, however. While both experiment and theory have focused on static, thermodynamic or at most linear-response quantities in the past, recently questions which explicitly involve the out-of-equilibrium time-dependence of such quantum systems have come to the foreground. These questions arise in the context of transport far from equilibrium or of decoherence, particularly as for very small devices mesoscopics and correlation physics merge. However, perhaps the most striking example is provided by the progress in preparing dilute ultracold bosonic and also fermionic alkali gases. Subjected to an optical lattice, these gases are arguably the purest realization of the typical model Hamiltonians of strong correlation physics, such as the Hubbard model [4, 5]. More importantly, the interaction parameters can be tuned experimentally on quantum mechanically relevant time-scales over a huge range, while being known precisely from microscopic calculations. From a theoretician's point of view, this situation is almost ideal, and has stimulated great interest in the development of time-dependent methods.

In this lecture, the emphasis is therefore also on recent extensions of DMRG into the real-time domain which make it the currently most powerful (and almost only) method for such problems: Following up on early attempts to extend DMRG to real-time, input from quantum information theory has led to the formulation of two DMRG algorithms for real-time evolutions [6–9]. As a “real-life” application, I focus on the real-time observation of the quintessential 1D phenomenon, spin-charge separation.

# 2 Density-matrix renormalization group

Let us start from the fundamental observation that key to the simulation of quantum systems is the mandatory and desirable compression of information: while the diverging number of degrees of freedom makes compression necessary on finite computing devices, compression also leads to the emergence of macroscopically meaningful concepts such as temperature and pressure which do not have microscopic counterparts. Yet, this divergence of degrees of freedom is of a different type for classical and quantum many-body systems: considering  $N$  spins on a lattice, the number of degrees of freedom diverges as  $2N$  (2 angles per spin) for a classical vector spin, which is polynomial in  $N$ , whereas it diverges as  $2^N$ , i.e. exponentially, for quantum spin-1/2. This is of course due to the presence of superpositions in quantum physics, making simulation exponentially harder.

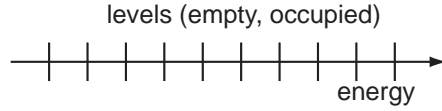


**Fig. 1:** *Quasi-one-dimensional arrangement of energy levels along the energy axis.*

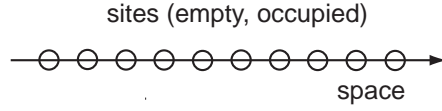


**Fig. 2:** *Local lattice degrees of freedom for a one-dimensional system.*

## 2.1 Decimation of state spaces

As quantum computers and simulators are not likely to be available in the immediate future, we are stuck to classical computers for the simulation of quantum systems. Essentially three strategies of dealing with the exponentially large state space are being followed: exact diagonalization deliberately limits itself to the exact study of small quantum systems, being limited to roughly 40 spins and 20 electrons. Stochastic techniques try to sample the state space efficiently; this is the realm of the quantum Monte Carlo methods, which however run into serious trouble for frustrated spins or fermionic systems due to the negative-sign problem. The last group of methods attempts a systematic choice of a subspace which is hoped to contain the physically most relevant states. This implies a physically driven process of discarding states, which I will refer to as decimation. All variational and renormalization group techniques are in this group, and the essential question is of course to identify the best decimation strategy which will depend both on the system and the question asked.

Let me focus on one particular, rather general decimation setup, “one-dimensional” decimation. Let us assume that the degrees of freedom can be arranged on a 1D axis, e.g. an energy axis, on which we place all levels, either empty or occupied, or a real-space axis, on which we place lattice sites (Figs. 1 and 2).

Imagine we grow the system iteratively towards the thermodynamic limit, adding site by site (whatever the physical interpretation of such a site will be) - Fig. 3. The original system, which I refer to as a block, is assumed to be effectively described within a state space  $\{|\alpha\rangle\}$  of dimension  $M$ , the new site within a state space  $\{|\sigma\rangle\}$  of dimension  $N$ . Obviously, the state space  $\{|\beta\rangle\}$  of the new block will have dimension  $MN$ , and for prevention of exponential growth it will be decimated down to dimension  $M$ . Whatever the physical decimation prescription will be, the states of the new block will be a linear combination of the old states,

$$|\beta\rangle = \sum_{\alpha} \sum_{\sigma} \langle \alpha \sigma | \beta \rangle |\alpha\rangle |\sigma\rangle. \quad (1)$$

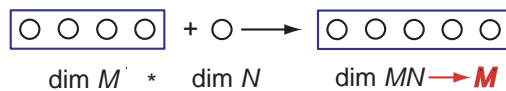


**Fig. 3:** *Growing a system: a local state space of dimension  $N$  is added to a block state space of dimension  $M$ .*

For later purposes, I will rewrite this expression as

$$|\beta\rangle = \sum_{\alpha} \sum_{\sigma} A_{\alpha\beta}[\sigma] |\alpha\rangle |\sigma\rangle, \quad (2)$$

where  $N$  matrices  $A$  of dimension  $M \times M$  have been introduced, one for each  $|\sigma\rangle$ , such that the matrix entries encode the expansion coefficients:  $A_{\alpha\beta}[\sigma] = \langle \alpha \sigma | \beta \rangle$ . From the orthonormality of the  $|\beta\rangle$  it follows that the  $A$ -matrices obey

$$\sum_{\sigma} A^{\dagger}[\sigma] A[\sigma] = 1. \quad (3)$$

Finding these matrix entries (i.e. decimating) in the optimal way is of course desirable; but before we try to formulate this as a well-posed problem, it is convenient to observe the following: the states of the block of length, say,  $\ell - 1$  serving as “input” to produce as “output” the states of the block of length  $\ell$  via the matrices  $A^{\ell}[\sigma_{\ell}]$ , are of course themselves the “output” for the construction of the block of length  $\ell - 1$  from that of  $\ell - 2$ , and so forth. We can therefore recursively write  $|\beta\rangle$  for a block of length  $\ell$  as

$$|\beta\rangle = \sum_{\sigma_1 \dots \sigma_{\ell}} [A^1[\sigma_1] A^2[\sigma_2] \dots A^{\ell}[\sigma_{\ell}]]_{\beta} |\sigma_1 \dots \sigma_{\ell}\rangle. \quad (4)$$

Obviously, for very short blocks, there are less than  $M$  states in a block, and the dimensions of the first  $A$ -matrices will be  $1 \times N$ ,  $N \times N^2$ ,  $\dots$  till  $M$  is exceeded. This turns the matrix product into a vector.

It is now convenient to consider also what happens if we start growing a chain from its right end (site  $L$ ). Obviously, similar expressions emerge: for a block of length  $\ell$  the states are given as

$$|\gamma\rangle = \sum_{\sigma_{L-\ell+1} \dots \sigma_L} [\tilde{A}^{L-\ell+1}[\sigma_{L-\ell+1}] \tilde{A}^{L-\ell+2}[\sigma_{L-\ell+2}] \dots \tilde{A}^L[\sigma_L]]_{\gamma} |\sigma_{L-\ell+1} \dots \sigma_L\rangle. \quad (5)$$

Again, at the chain end the  $\tilde{A}$  matrices (defined in analogy to the  $A$ ) have reduced dimensions instead of  $M \times M$ ; there is also a slightly modified orthonormality constraint,

$$\sum_{\sigma} \tilde{A}[\sigma] \tilde{A}^{\dagger}[\sigma] = 1. \quad (6)$$

We may now choose a “left” and a “right” block to join them to the generic description of a quantum state of the system of length  $L$ , matching them directly,

$$|\psi\rangle = \sum_{\sigma_1 \dots \sigma_L} A^1[\sigma_1] \dots A^{\ell}[\sigma_{\ell}] \Psi \tilde{A}^{\ell+1}[\sigma_{\ell+1}] \dots \tilde{A}^L[\sigma_L] |\sigma_1 \dots \sigma_L\rangle, \quad (7)$$

where  $\Psi$  is a  $M \times M$  matrix, or with one site explicitly in between,

$$|\psi\rangle = \sum_{\sigma_1 \dots \sigma_L} A^1[\sigma_1] \dots A^{\ell}[\sigma_{\ell}] \Psi[\sigma_{\ell+1}] \tilde{A}^{\ell+2}[\sigma_{\ell+2}] \dots \tilde{A}^L[\sigma_L] |\sigma_1 \dots \sigma_L\rangle, \quad (8)$$

where there is a  $\Psi$ -matrix for each  $|\sigma_{\ell+1}\rangle$ , or with two sites explicitly in between,

$$|\psi\rangle = \sum_{\sigma_1 \dots \sigma_L} A^1[\sigma_1] \dots A^{\ell}[\sigma_{\ell}] \Psi[\sigma_{\ell+1} \sigma_{\ell+2}] \tilde{A}^{\ell+3}[\sigma_{\ell+3}] \dots \tilde{A}^L[\sigma_L] |\sigma_1 \dots \sigma_L\rangle. \quad (9)$$

As it turns out, Eqns. (8) and (9) are the useful ones – both of them highlighting different aspects of DMRG, leading to what is called single-site and (more conventional) two-site DMRG.

Considering Eq. (7), obviously the junction can be shifted freely, even ficticiously to the right end of the chain, with all  $\tilde{A}$ -matrices disappearing. The generic description of a quantum state emerging from a decimation procedure is therefore given by

$$|\psi\rangle = \sum_{\sigma_1 \dots \sigma_L} A^1[\sigma_1] A^2[\sigma_2] \dots A^L[\sigma_L] |\sigma_1 \dots \sigma_L\rangle. \quad (10)$$

In fact, there is no need to worry about this product of matrices yielding a scalar factor because of the dimension of the matrices at the right end: manipulations introduced further down (namely the Schmidt decomposition) can be used to show that without any loss the  $A$ -matrices shrink to dimensions mirroring those at the left end, e.g.  $N^2 \times N$  and  $N \times 1$  for the last two. The generic decimation state encoded as in Eq. (10) is referred to as a *matrix product state*; such states have been studied for a long time [10–12].

Again, the  $A$ -matrices encode the physical decimation prescription, and we may now specify our question, what is the optimal decimation prescription, for the case of finding the *ground state* of a Hamiltonian. Clearly the answer is to find the prescription yielding those  $A$  that minimize  $\langle \psi | \hat{H} | \psi \rangle$  assuming normalization. Working out this expression yields a highly non-linear expression for the energy in  $A$ , which is numerically close on useless.

Can we find a method that does turns this into a linear problem in  $A$ , which would be much easier to implement in a stable way on a computer? In fact, we can, and this has already been done in the past in the form of the density-matrix renormalization group [1–3]. Its link to matrix product states has been pointed out by various authors [13–16]. As there are many reviews of DMRG following a traditional way of understanding (e.g. [3]), going to more depth than possible here, I want to present a different viewpoint of the method as an answer to the question above.

A way of turning the problem linear would consist, roughly speaking, in providing some starting set of matrices in a warm-up procedure, preferably close to the true solution, and then to proceed iteratively: keeping all elements (i.e. matrices) in  $|\psi\rangle$  fixed, with one exception,  $\langle \psi | \hat{H} | \psi \rangle$  turns quadratic in the free matrix, and extremizing this expression with respect to the free matrix is a linear procedure. Varying one element after another repeatedly, one may hope to get a very good, even optimal, approximation of the ground state within the state class expressible as above.

In standard DMRG language, the first warm-up part of the procedure would correspond to the so-called infinite-system algorithm, the second to the finite-system algorithm, which is the true cornerstone of the method. As the infinite-system algorithm is described very well in many references, and one may even imagine starting from random matrices, I will focus on the finite-system algorithm.

## 2.2 Finite-system DMRG procedures

*Two-site DMRG.* Let us consider we have our quantum state in the representation of Eq. (9). In that case, the left block of length  $\ell$  formed from  $A$ -matrices would be described by a  $M$ -dimensional Hilbert space with states  $\{|m_\ell^S\rangle\}$  defined as in Eq. (4); similarly the right block of length  $L - \ell - 2$  by states  $\{|m_{L-\ell-2}^E\rangle\}$ . In both cases, we assume that we know all necessary operators on the blocks in these effective bases. We can therefore construct the Hamiltonian

acting on

$$\begin{aligned}
 |\psi\rangle &= \sum_{m^S=1}^M \sum_{\sigma^S=1}^N \sum_{\sigma^E=1}^N \sum_{m^E=1}^M \Psi_{m^S m^E} [\sigma^S \sigma^E] |m^S \sigma^S\rangle |m^E \sigma^E\rangle \\
 &\equiv \sum_i^{N^S} \sum_j^{N^E} \Psi_{ij} |i\rangle |j\rangle; \quad \langle \psi | \psi \rangle = 1,
 \end{aligned} \tag{11}$$

where  $\Psi_{m^S m^E} [\sigma^S \sigma^E] = \langle m^S \sigma^S; \sigma^E m^E | \psi \rangle$ .  $\{|m^S \sigma^S\rangle\} \equiv \{|i\rangle\}$  and  $\{|m^E \sigma^E\rangle\} \equiv \{|j\rangle\}$ . The state spaces  $\{|i\rangle\}$  and  $\{|j\rangle\}$  have dimensions  $N^S = MN$  and  $N^E = MN$ . Using some large sparse matrix solver one may minimize the energy of  $|\psi\rangle$  with respect to  $\Psi_{ij}$ .

In order to make progress, we now have to shift the position of the two active sites, to improve our wave function everywhere. If we shift it by one site to the right, the shrinking right block may easily be constructed from  $\tilde{A}$ -matrices; for the growing left block, we have to provide  $A$ -matrices for the left of the two sites (states  $|\sigma^S\rangle$ ). If one has a suitable truncation of the basis  $\{|i\rangle\}$  down to  $M$  states, their expansion in  $|m^S\rangle$  and  $|\sigma^S\rangle$  will just define the desired  $A$ -matrices. To find that truncation, a useful concept is that of a *Schmidt decomposition*: Consider a quantum state  $|\psi\rangle = \sum_{ij} \psi_{ij} |i\rangle \otimes |j\rangle$  as introduced before, with  $N^S$  states  $|i\rangle$  and  $N^E$  states  $|j\rangle$ . Assuming without loss of generality  $N^S \geq N^E$ , we form the  $(N^S \times N^E)$ -dimensional matrix  $A$  with  $A_{ij} = \psi_{ij}$ . Singular value decomposition guarantees  $A = U D V^T$ , where  $U$  is  $(N^S \times N^E)$ -dimensional with orthonormal columns,  $D$  is a  $(N^E \times N^E)$ -dimensional diagonal matrix with non-negative entries  $D_{\alpha\alpha} = \sqrt{w_\alpha}$ , and  $V^T$  is a  $(N^E \times N^E)$ -dimensional unitary matrix;  $|\psi\rangle$  can be written as

$$\begin{aligned}
 |\psi\rangle &= \sum_{i=1}^{N^S} \sum_{\alpha=1}^{N^E} \sum_{j=1}^{N^E} U_{i\alpha} \sqrt{w_\alpha} V_{\alpha j}^T |i\rangle |j\rangle \\
 &= \sum_{\alpha=1}^{N^E} \sqrt{w_\alpha} \left( \sum_{i=1}^{N^S} U_{i\alpha} |i\rangle \right) \left( \sum_{j=1}^{N^E} V_{\alpha j} |j\rangle \right).
 \end{aligned} \tag{12}$$

The orthonormality properties of  $U$  and  $V^T$  ensure that  $|w_\alpha^S\rangle = \sum_i U_{i\alpha} |i\rangle$  and  $|w_\alpha^E\rangle = \sum_j V_{\alpha j} |j\rangle$  form orthonormal bases of system and environment respectively, in which the Schmidt decomposition

$$|\psi\rangle = \sum_{\alpha=1}^{N_{\text{Schmidt}}} \sqrt{w_\alpha} |w_\alpha^S\rangle |w_\alpha^E\rangle \tag{13}$$

holds.  $N^S N^E$  coefficients  $\psi_{ij}$  are reduced to  $N_{\text{Schmidt}} \leq N^E$  non-zero coefficients  $\sqrt{w_\alpha}$ ,  $w_1 \geq w_2 \geq w_3 \geq \dots$ . Relaxing the assumption  $N^S \geq N^E$ , one has

$$N_{\text{Schmidt}} \leq \min(N^S, N^E). \tag{14}$$

Upon tracing out environment or system the reduced density matrices for system and environment are found to be

$$\hat{\rho}_S = \sum_{\alpha}^{N_{\text{Schmidt}}} w_\alpha |w_\alpha^S\rangle \langle w_\alpha^S|; \quad \hat{\rho}_E = \sum_{\alpha}^{N_{\text{Schmidt}}} w_\alpha |w_\alpha^E\rangle \langle w_\alpha^E|. \tag{15}$$

Analyzing reduced density matrices or the Schmidt decomposition therefore yield exactly the same information. This fact was understood from the very beginning of DMRG, although DMRG people were not aware of the term “Schmidt decomposition”. In fact, the singular value decomposition representation of the wavefunction was understood before the density matrix representation. How can we put this information to good use? Interestingly enough, it allows us to define several physically motivated truncation criteria, that lead to the identical truncation prescription.

*Optimization of the wave function:* Quantum mechanical objects are completely described by their wave function. It is thus a reasonable demand for a truncation procedure that the approximative wave function  $|\tilde{\psi}\rangle$  where the system space has been truncated to be spanned by only  $M$  orthonormal states  $|\alpha\rangle = \sum_i u_{\alpha i} |i\rangle$ ,

$$|\tilde{\psi}\rangle = \sum_{\alpha=1}^M \sum_{j=1}^{N^E} a_{\alpha j} |\alpha\rangle |j\rangle, \quad (16)$$

minimizes the distance in the quadratic norm

$$\| |\psi\rangle - |\tilde{\psi}\rangle \| . \quad (17)$$

Using Eq. (13), one finds that this distance is minimized if one *retains the  $M$  eigenstates of  $\hat{\rho}_S$  with the largest eigenvalues  $w_\alpha$* . This is the key truncation prescription.

One could also ask for maximizing the retained *bipartite entanglement* between system and environment under truncation. As bipartite entanglement is defined as  $S = -\sum_\alpha w_\alpha \log_2 w_\alpha$ , and that typically one has a large number of relatively small eigenvalues, this again leads to the same truncation prescription, and the method preserves entanglement as well as it can.

Interestingly enough, one can show that the (additional) error introduced by truncation on some generic bounded operator  $\hat{A}$  acting on the system, such as the energy per lattice bond,  $\|\hat{A}\| = \max_\phi |\langle \phi | \hat{A} | \phi \rangle| / |\langle \phi | \phi \rangle| \equiv c_A$ , is minimized by the above procedure. This error for  $\langle \hat{A} \rangle$  is bounded by

$$|\langle \hat{A} \rangle_{\text{approx}} - \langle \hat{A} \rangle| \leq \left( \sum_{\alpha > M}^{MN} w_\alpha \right) c_A \equiv \epsilon_\rho c_A, \quad (18)$$

neglecting a small normalization correction. For local quantities, such as energy, magnetization or density, errors are of the order of the *truncated weight*

$$\epsilon_\rho = 1 - \sum_{\alpha=1}^M w_\alpha, \quad (19)$$

which emerges as the key estimate. Careful extrapolation of results in  $M$  (better  $\epsilon_\rho$ ) is therefore highly recommended.

Collecting these ideas, the so-called *finite-system DMRG algorithm* can now be formulated (Fig. 4). For a one-dimensional lattice of total length  $L$ :

1. Consider a (left) system block S of length  $\ell$ . S lives on a Hilbert space of size  $M$  with states  $\{|m_\ell^S\rangle\}$ ; the Hamiltonian  $\hat{H}_\ell^S$  and the operators acting on the block are assumed to be known in this basis. Similarly, we have a (right) environment block E of size  $L - \ell - 2$ .

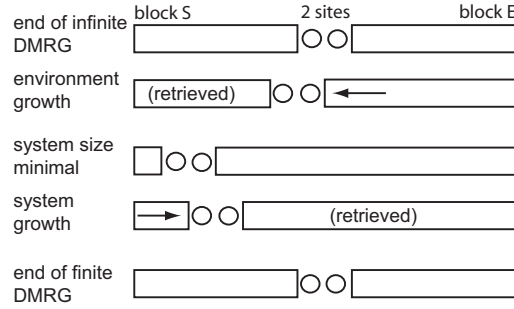


**Fig. 4:** *Finite-system DMRG algorithm. Block growth and shrinkage. For the adaptive time-dependent DMRG, ground state optimization in this setup will be replaced by a local time evolution on the two sites.*

2. Build the total system (superblock) of length  $L$  from S, E and two sites in between. S and the left site live on a Hilbert space of size  $N^S = MN$ , with a basis of product states  $\{|m_\ell^S \sigma^S\rangle\}$ . Similarly, environment and the right site are joined. The total Hilbert space is of size  $N^S N^E$ , and a total Hamiltonian can be constructed.
3. Find by large sparse-matrix diagonalization of the total Hamiltonian the ground state  $|\psi\rangle$ . This is the most time-consuming part of the algorithm. For better performance, there is a simple, but powerful “prediction algorithm” [17], which cuts down calculation times in finite-system DMRG by more than an order of magnitude. Using the  $A$ -matrices, it transforms  $|\psi\rangle$  from the last step approximatively into the new basis and uses it as guess for the next, improved  $|\psi\rangle$ .
4. Form the reduced density-matrix  $\hat{\rho} = \text{Tr}_E |\psi\rangle\langle\psi|$  and determine its eigenbasis  $|w_\alpha\rangle$  ordered by descending eigenvalues (weight)  $w_\alpha$ . Form a new (reduced) basis for S and the left site by taking the  $M$  eigenstates with the largest weights, defining the  $A$ -matrices for this site. Proceed likewise for the environment.
5. Form a new system block from S and one added site. As environment block, use the one shorter than E by one site. This effectively shifts the free sites by one to the right.
6. Carry out the reduced basis transformations of needed operators onto the new  $M^S$ -state basis. Restart with step (2) with block size  $\ell + 1$  until the right end of the chain is reached.
7. Continue the above procedure with system and environment in reversed roles, the free sites being shifted left, until the left end is reached, and so forth, until results are converged. A complete shrinkage and growth sequence for both blocks is called a *sweep*.

DMRG practitioners usually adopt a quite pragmatic approach when applying DMRG to study some physical system. They consider the convergence of DMRG results under tuning the standard DMRG control parameters, system size  $L$ , size of the reduced block Hilbert space  $M$ , and the number of finite-system sweeps, and judge DMRG results to be reliable or not.

*Single site DMRG.* In practical applications one observes that even for translationally invariant systems with periodic boundary conditions and repeated applications of finite-system sweeps the position dependency of the matrix-product state (or of observables) does not go away completely as it strictly should, indicating room for further improvement. Also, the method cannot be strictly variational: the ansatz (9) generates (after the Schmidt decomposition and before



truncation) ansatz matrices of dimension  $MN$  at the two local sites due to Eq. (14), whereas they are of dimension  $M$  at all other sites; as the position of these two sites is shifting, this anomaly changes place such that one is not really optimizing within one fixed variational ansatz throughout the algorithm.

Several authors [14, 15] have pointed out and numerically demonstrated that DMRG results can be improved by switching, after convergence is reached, from the  $S\bullet\bullet E$  scheme for the finite-system algorithm to a  $S\bullet E$  scheme as in ansatz (8) and to carry out some more sweeps. This is now a truly variational ansatz [14–16]:

In the new scheme the ansatz matrix  $\Psi$  can be projected down to finding  $M$  states for defining the  $A$ -matrix without truncation or loss of information or change in energy, because the Schmidt number of non-zero contributions to the density matrix cannot exceed  $M$ , which is the dimension of the environment in Eq. (14) for the single-site setup. Shifting the “active” site then does not change the energy, and the next minimization can only decrease the energy (or keep it constant). This setup is therefore truly variational in the space of the states generated by the matrices  $A$ ,  $\tilde{A}$  and reaches a minimum of energy within that space. It is important to note that in this setup there is therefore no truncation error as diagnostic tool.

There is of course no guarantee to reach the global minimum: in fact, it turns out that an immediate application of the formally superior single site DMRG may fail quite drastically by trapping, but this can be mended by suitable modifications to the state selection scheme, taking the state out of false minima [18].

### 2.3 When and why does DMRG work?

Obviously, the ordered eigenvalue spectrum  $w_\alpha$  of the reduced density-matrix  $\hat{\rho}$  should decay as quickly as possible to minimize the truncated weight  $\epsilon_\rho = 1 - \sum_{\alpha=1}^M w_\alpha$  for optimal DMRG performance. The optimal case is of course when the state to be approximated is a one-dimensional  $M \times M$  *matrix-product state*, which can be modelled exactly. More generally, in one dimension, density-matrix spectra of gapped one-dimensional quantum systems exhibit roughly system-size independent exponential decay of  $w_\alpha$ ; at criticality, this decay slows down with increasing system size, leading to DMRG failure for  $L \rightarrow \infty$ . In two dimensions, in reduced density-matrix spectra for states of systems both at and away from criticality, the number of eigenvalues to be retained to keep a fixed truncation error grows exponentially with system size, restricting DMRG to very small system sizes (typically, the two-dimensional lattice is mapped to a one-dimensional snake with long-ranged interactions).

These empirical observations can be understood from examining the growth of bipartite entanglement between system and environment for various dimensions. Consider the entanglement  $S_L$  for systems of length  $L$  embedded in a thermodynamic limit universe. One finds [19] that  $S_L \rightarrow \infty$  for  $L \rightarrow \infty$  at criticality, but saturates as  $S_L \rightarrow S_L^*$  for  $L \approx \xi$  in the non-critical regime. At criticality the entanglement can be linked [19, 20] to the geometric entropy [21] of associated conformal field theories,

$$S_L^{geo} = \frac{c + \bar{c}}{6} \log_2 L, \quad (20)$$

where  $c$  ( $\bar{c}$ ) are the central charges. As examples, for the anisotropic XY model  $c = \bar{c} = 1/2$  and for the Heisenberg model and isotropic XY model  $c = \bar{c} = 1$ .

Geometric entropy arguments for  $(d + 1)$ -dimensional field theories use a bipartition of  $d$ -dimensional space by a  $(d - 1)$ -dimensional hypersurface, which is shared by system  $S$  and

environment E. By the Schmidt decomposition, S and E share the same reduced density-matrix spectrum, hence entanglement entropy, which is now argued to reside essentially on the shared hypersurface; see also [22]. Taking the thermodynamic (infrared) limit, entropy scales as the hypersurface area,

$$S_L \propto \left(\frac{L}{\lambda}\right)^{d-1}, \quad (21)$$

where  $\lambda$  is some ultraviolet cutoff which in condensed matter physics we may fix at some lattice spacing; critical systems will have logarithmic corrections to (21).

$S_L$  is the number of qubits corresponding to the entanglement information. To code this information in DMRG, one needs a system Hilbert space of size  $M \geq 2^{S_L}$ , we may therefore expect, in perfect agreement with empirical results, that in 1D quantum systems away from criticality, DMRG yields very precise results for the TD limit for some finite number of states kept,  $M \sim 2^{S_L^*}$ . At criticality, the number of states that has to be kept, will diverge as

$$M(L) \sim L^k, \quad (22)$$

with  $k$  inferred from Eq. (20). This explains the failure of DMRG for critical one-dimensional systems as  $L \rightarrow \infty$ . As  $k$  is small, this statement has to be qualified; DMRG still works for rather large finite systems.

In higher-dimensional quantum systems, however, the number of states to be kept will diverge as

$$M(L) \sim 2^{L^{d-1}}, \quad (23)$$

rendering the understanding of thermodynamic limit behavior by conventional DMRG quite impossible. In any case, even for higher-dimensional systems, DMRG may be a very useful method as long as system size is kept resolutely finite, such as in nuclear physics or quantum chemistry applications. Recent proposals [23] also show that it is possible to formulate generalized DMRG ansatz states in such a way that entropy shows correct size dependency in two-dimensional systems.

### 3 Time-dependence in quantum systems

Even though the methods described in the previous section provide high-quality linear-response quantities, they fail in truly out-of-equilibrium situations or for time-dependent Hamiltonians. It has therefore been of high interest to find DMRG approaches dealing with state evolution in real-time.

To see the advantages of such an approach, consider the following. Essentially all physical quantities of interest involving time can be reduced to the calculation of either *equal-time*  $n$ -point correlators such as the (1-point) density

$$\langle n_i(t) \rangle = \langle \psi(t) | n_i | \psi(t) \rangle = \langle \psi | e^{i\hat{H}t} n_i e^{-i\hat{H}t} | \psi \rangle \quad (24)$$

or *unequal-time*  $n$ -point correlators such as the (2-point) real-time Green's function

$$G_{ij}(t) = \langle \psi | c_i^\dagger(t) c_j(0) | \psi \rangle = \langle \psi | e^{+i\hat{H}t} c_i^\dagger e^{-i\hat{H}t} c_j | \psi \rangle. \quad (25)$$

This expression can be cast in a form very close to Eq. (24) by introducing  $|\phi\rangle = c_j|\psi\rangle$  such that the desired correlator is then simply given as an equal-time matrix element between two time-evolved states,

$$G_{ij}(t) = \langle \psi(t) | c_i^\dagger | \phi(t) \rangle. \quad (26)$$

If both  $|\psi(t)\rangle$  and  $|\phi(t)\rangle$  can be calculated, a very appealing feature of this approach is that  $G_{ij}(t)$  can be evaluated in *a single calculation* for all  $i$  and  $t$  as time proceeds. Frequency-momentum space is then reached by a double Fourier transformation. Obviously, finite system-sizes and edge effects as well as algorithmic constraints will impose physical constraints on the largest times and distances  $|i-j|$  or minimal frequency and wave vectors resolutions accessible. Nevertheless, this approach might emerge as a very attractive alternative to the current very time-consuming calculations of  $G(k, \omega)$  using the dynamical DMRG [24, 25].

The fundamental difficulty of obtaining the above correlators becomes obvious if we examine the time-evolution of the quantum state  $|\psi(t=0)\rangle$  under the action of some (for simplicity) time-independent Hamiltonian  $\hat{H}|\psi_n\rangle = E_n|\psi_n\rangle$ . If the eigenstates  $|\psi_n\rangle$  are known, expanding  $|\psi(t=0)\rangle = \sum_n c_n |\psi_n\rangle$  leads to the well-known time evolution

$$|\psi(t)\rangle = \sum_n c_n \exp(-iE_n t) |\psi_n\rangle, \quad (27)$$

where the modulus of the expansion coefficients of  $|\psi(t)\rangle$  is time-independent. A sensible Hilbert space truncation is given by a projection onto the large-modulus eigenstates. In strongly correlated systems, however, we usually have no good knowledge of the eigenstates. Instead, one uses some orthonormal basis with unknown eigenbasis expansion,  $|k\rangle = \sum_n a_{kn} |\psi_n\rangle$ . The time evolution of the state  $|\psi(t=0)\rangle = \sum_k d_k(0) |k\rangle$  then reads

$$|\psi(t)\rangle = \sum_k \left( \sum_n d_k(0) a_{kn} e^{-iE_n t} \right) |k\rangle \equiv \sum_k d_k(t) |k\rangle, \quad (28)$$

where the modulus of the expansion coefficients  $d_k(t)$  is *time-dependent*. For a general orthonormal basis, Hilbert space truncation at one fixed time (i.e.  $t=0$ ) will therefore not ensure a reliable approximation of the time evolution. Also, energy *differences* matter in time evolution due to the phase factors  $e^{-i(E_n - E_{n'})t}$  in  $|d_k(t)|^2$ . Thus, a good approximation to the low-energy Hamiltonian alone (as provided by DMRG) is of limited use.

## 4 Early attempts in DMRG

Cazalilla and Marston [26] were the first to exploit DMRG to systematically calculate time-dependent quantum many-body effects. They studied a time-dependent Hamiltonian  $\hat{H}(t) \equiv \hat{H}(0) + \hat{V}(t)$ , where  $\hat{V}(t)$  encodes the time-dependent part of the Hamiltonian. After applying a standard DMRG calculation to the Hamiltonian  $\hat{H}(t=0)$ , the time-dependent Schrödinger equation was numerically integrated forward in time. The effective Hamiltonian in the reduced Hilbert space was built as  $\hat{H}_{\text{eff}}(t) = \hat{H}_{\text{eff}}(0) + \hat{V}_{\text{eff}}(t)$ , where  $\hat{H}_{\text{eff}}(0)$  was taken as the last superblock Hamiltonian approximating  $\hat{H}(0)$ .  $\hat{V}_{\text{eff}}(t)$  as an approximation to  $\hat{V}$  was built using the representations of operators in the final block bases. The initial condition was obviously to take  $|\psi(0)\rangle$  as the ground state obtained by the preliminary DMRG run. This procedure amounts to working within a *static* reduced Hilbert space, namely that optimal at  $t=0$ , and projecting all wave functions and operators onto it.

In this approach the hope is that an effective Hamiltonian obtained by targeting the ground state of the  $t=0$  Hamiltonian is capable to catch the states that will be visited by the time-dependent Hamiltonian during time evolution. This approach must however break down after relatively short times as the full Hilbert space is explored, as became quickly obvious.

*Dynamic time-dependent DMRG.* Several attempts have been made to improve on static time-dependent DMRG by enlarging the reduced Hilbert space using information on the time-evolution, such that the time-evolving state has large support on that *dynamic* Hilbert space for longer times. Whatever procedure for enlargement is used, the problem remains that the number of DMRG states  $m$  grows with the desired simulation time as they have to encode more and more different physical states. As DMRG calculation time scales as  $M^3$  (due to the matrix-matrix multiplications involved), this type of approach will meet its limitations somewhat later in time. All enlargement procedures rest on the ability of DMRG to describe – at some numerical expense – small sets of states (“target states”) very well instead of just one.

The first approach has been demonstrated by Luo, Xiang and Wang [27]. They use a density matrix that is given by a superposition of states  $|\psi(t_i)\rangle$  at various times of the evolution,  $\hat{\rho} = \sum_{i=0}^{N_t} \alpha_i |\psi(t_i)\rangle \langle \psi(t_i)|$  with  $\sum \alpha_i = 1$  for the determination of the reduced Hilbert space. Of course, these states are not known initially; it was proposed by them to start within the framework of infinite-system DMRG from a small DMRG system and evolve it in time. For a very small system this procedure is exact. For this system size, the state vectors  $|\psi(t_i)\rangle$  are used to form the density matrix. This density matrix then determines the reduced Hilbert space for the next larger system, taking into account how time-evolution explores the Hilbert space for the smaller system. One then moves on to the next larger DMRG system where the procedure is repeated. This is of course very time-consuming.

Schmitteckert [28] has computed the transport through a small interacting nanostructure using an Hilbert space enlarging approach, based on the time evolution operator. To this end, he splits the problem into two parts: By obtaining a relatively large number of low-lying eigenstates exactly (within time-independent DMRG precision), one can calculate their time evolution exactly. For the subspace orthogonal to these eigenstates, he implements the matrix exponential  $|\psi(t+\Delta t)\rangle = \exp(-i\hat{H}\Delta t)|\psi(t)\rangle$  using the Krylov subspace approximation. For any block-site configuration during sweeping, he evolves the state in time, obtaining  $|\psi(t_i)\rangle$  at fixed times  $t_i$ . These are targeted in the density matrix, such that upon sweeping forth and back a Hilbert space suitable to describe all of them at good precision should be obtained. For numerical efficiency, he carries out this procedure to convergence for some small time, which is then increased upon sweeping, bringing more and more states  $|\psi(t_i)\rangle$  into the density matrix. Again, this is a very time-consuming approach.

## 5 Adaptive time-dependent DMRG

Decisive progress came from an unexpected corner, namely quantum information theory, when Vidal proposed an algorithm for simulating quantum time evolutions of one-dimensional systems efficiently on a classical computer [6, 29]. His algorithm, known as TEBD [time-evolving block decimation] algorithm, is based on matrix product states [11, 12]; as it turned out, it is so closely linked to DMRG concepts, that his ideas could be implemented easily into DMRG, leading to an *adaptive* time-dependent DMRG [7, 8], where the DMRG state space adapts itself in time to the time-evolving quantum state. One immediately profits from all the DMRG development for exploiting good quantum numbers and other speed-ups.

If we consider a nearest-neighbor Hamiltonian, such as the conventional Hubbard Hamiltonian, we can split the infinitesimal global time evolution operator into a product of infinitesimal local time evolution operators [30]:

$$e^{-i\hat{H}\Delta t} = e^{-ih_1\Delta t} e^{-ih_2\Delta t} e^{-ih_3\Delta t} \dots e^{-ih_{L-1}\Delta t} + O(\Delta t^2). \quad (29)$$

The  $h_i$  are the local Hamiltonians acting on bonds  $i$ ; in general only odd and even bond Hamiltonians will commute in their groups, giving rise to an error in the decomposition. The idea is now simply to use finite-system DMRG in the two-site setup: at each step, one carries out the local infinitesimal time evolution exactly on the two adjacent local sites. This will lead to a new state, a new Schmidt decomposition carried is out in which the system is cut between the two local sites, as before, leading to a new truncation and new reduced basis transformations (2 matrices  $A$  adjacent to this bond), which are the choice optimally representing the new state. By doing this for all bonds, one infinitesimal time step is completed.

To do this, one needs the wave function  $|\psi\rangle$  in a two-block two-site configuration such that the bond that is currently updated consists of the two free sites. This implies that  $|\psi\rangle$  has to be transformed between different configurations. As mentioned above, in finite-system DMRG such a transformation, which was first implemented by White [17] (“state prediction”) is routinely used to predict the outcome of large sparse matrix diagonalizations, which no longer occur during time evolution. Here, it merely serves as a basis transformation.

The adaptive time-dependent DMRG algorithm which incorporates the TEBD simulation algorithm in the DMRG framework is therefore set up as follows:

0. Set up a conventional finite-system DMRG algorithm with state prediction using the Hamiltonian at time  $t = 0$ ,  $\hat{H}(0)$ , to determine the ground state of some system of length  $L$  using effective block Hilbert spaces of dimension  $M$ . At the end of this stage of the algorithm, we have for blocks of all sizes  $l$  reduced orthonormal bases spanned by states  $|m_l\rangle$ , which are characterized by good quantum numbers. Also, we have all reduced basis transformations, corresponding to the matrices  $A$ .
1. For each Trotter time step, use the finite-system DMRG algorithm to run one sweep with the following modifications:
  - i) For each even bond apply the local time evolution  $\hat{U}$  at the bond formed by the free sites to  $|\psi\rangle$ . This is a very fast operation compared to determining the ground state, which is usually done instead in the finite-system algorithm.
  - ii) As always, perform a DMRG truncation at each step of the finite-system algorithm, hence  $O(L)$  times.
  - iii) Use White’s prediction method to get the representation of the time-evolved state in the setup with the free sites shifted by one.
2. In the reverse direction, apply step (i) to all odd bonds.
3. As in standard finite-system DMRG evaluate operators when desired at the end of some time steps. Note that there is no need to generate these operators at all those time steps where no operator evaluation is desired, which will, due to the small Trotter time step, be the overwhelming majority of steps.

Note that one can also perform every bond evolution operator at each half-sweep, in order. This does not worsen the Trotter error, since in the reverse sweep the operators are applied in reverse order.

The calculation time of adaptive time-dependent DMRG scales linearly in  $L$ , as opposed to the static time-dependent DMRG which does not depend on  $L$ . The diagonalization of the density matrices (Schmidt decomposition) scales as  $N^3 M^3$ ; the preparation of the local time

evolution operator as  $N^6$ , but this may have to be done only rarely e.g. for discontinuous changes of interaction parameters. Carrying out the local time evolution scales as  $N^4 M^2$ ; the basis transformation scales as  $N^2 M^3$ . As  $M \gg N$  typically, the algorithm is of order  $O(LN^3 M^3)$  at each time step.

The performance of this method has been tested in various applications in the context of ultra-cold atom physics [7, 31–33], but also for far-from-equilibrium dynamics [34] and for spectral functions [8]; some of these applications will serve as examples in the following.

Before we move on, it should be mentioned that this method for time evolution, while very fast, has weaknesses due to its usage of the Trotter decomposition: first and not so important, there is the Trotter decomposition error depending on the time step. The Trotter error is small and can be reduced to negligible levels by using higher order Trotter decompositions – we are currently using mostly 4th order. More importantly, they are limited to systems with nearest neighbor interactions on a single chain; this problem can be circumvented by introducing larger unit cells such that interactions become nearest neighbor again – given the scaling in  $N$ , this is not very feasible. A better approach in such cases is to use the time-step targetted method [9] which, at quite some algorithmic cost in time, does not have these limitations. The main idea is to produce a basis which targets the states needed to represent one small but finite time step. Once this basis is complete enough, the time step is taken and the algorithm proceeds to the next time step. This targetting is intermediate to the other approaches: the Trotter methods target precisely one instant in time at any DMRG step, while Luo, Xiang, and Wang’s approach [27] considered the entire range of time to be studied. For the subtle details, I refer to [9].

## 6 Error analysis: magnetization dynamics

In this section, we consider the dynamics of a system far from equilibrium using adaptive time-dependent DMRG [34]. The following example, for which an exact solution is available, shows that time-dependent DMRG can also perform in situations where dynamical DMRG must surely fail. The exact solution allows us DMRG-independent error analysis.

The initial state  $|\text{ini}\rangle = |\uparrow \dots \uparrow \downarrow \dots \downarrow\rangle$  on a one-dimensional spin-1/2 chain is subjected to the dynamics of the Heisenberg model

$$H = \sum_n S_n^x S_{n+1}^x + S_n^y S_{n+1}^y + J_z S_n^z S_{n+1}^z \equiv \sum_n h_n. \quad (30)$$

We set  $\hbar = 1$ , defining time to be 1/energy with the energy unit chosen as the  $J_{xy}$  interaction. The case  $J_z = 0$  describes equivalently free fermions on a lattice, and can be solved exactly. In the following we will focus on this case. Note that in that case the initial state with two large ferromagnetic domains separated by a domain wall in the center is a highly excited state; the ground state exhibits power-law decaying antiferromagnetic correlations.

The time evolution delocalizes the domain wall over the entire chain; the magnetization profile for the initial state  $|\text{ini}\rangle$  reads [35]:

$$S_z(n, t) = \langle \psi(t) | S_n^z | \psi(t) \rangle = -1/2 \sum_{j=1-n}^{n-1} J_j^2(t), \quad (31)$$

where  $J_j$  is the Bessel function of the first kind.  $n = \dots, -3, -2, -1, 0, 1, 2, 3, \dots$  labels chain sites with the convention that the first site in the right half of the chain has label  $n = 1$ . As the

total energy of the system is conserved, the state cannot relax to the ground state. The exact solution reveals a nontrivial behaviour with a complicated substructure in the magnetization profile, which is a good benchmark for DMRG.

*Possible errors.* Two main sources of error occur in the adaptive t-DMRG:

(i) The *Trotter error* due to the Trotter decomposition. For an  $n$ th-order Trotter decomposition [30], the error made in one time step  $dt$  is of order  $Ldt^{n+1}$ . To reach a given time  $t$  one has to perform  $t/dt$  time-steps, such that in the worst case the error grows linearly in time  $t$  and the resulting error is of order  $L(dt)^nt$ .

(ii) The DMRG *truncation error* due to the representation of the time-evolving quantum state in reduced (albeit “optimally” chosen) Hilbert spaces and to the repeated transformations between different truncated basis sets. While the truncation error  $\epsilon$  that sets the scale of the error of the wave function and operators is typically very small, here it will strongly accumulate as  $O(Lt/dt)$  truncations are carried out up to time  $t$ . This is because the truncated DMRG wave function has norm less than one and is renormalized at each truncation by a factor of  $(1-\epsilon)^{-1} > 1$ . Truncation errors should therefore accumulate roughly exponentially with an exponent of  $\epsilon Lt/dt$ , such that eventually the adaptive t-DMRG will break down at too long times. The accumulated truncation error should decrease considerably with an increasing number of kept DMRG states  $M$ . For a fixed time  $t$ , it should decrease as the Trotter time step  $dt$  is increased, as the number of truncations decreases with the number of time steps  $t/dt$ .

At this point, it is worthwhile to mention that our subsequent error analysis should also be pertinent to the very closely related time-evolution algorithm introduced by Verstraete *et al.* [44], which also involves both Trotter and truncation errors.

We remind the reader that no error is encountered in the application of the local time evolution operator  $U_n$  to the state  $|\psi\rangle$ .

*Error analysis.* We use two main measures for the error:

(i) As a measure for the overall error we consider the *magnetization deviation*, the maximum deviation of the local magnetization found by DMRG from the exact result,

$$\text{err}(t) = \max_n |\langle S_{n,\text{DMRG}}^z(t) \rangle - \langle S_{n,\text{exact}}^z(t) \rangle|. \quad (32)$$

(ii) As a measure which excludes the Trotter error we use the *forth-back deviation*  $FB(t)$ , which we define as the deviation between the initial state  $|\text{ini}\rangle$  and the state  $|fb(t)\rangle = U(-t)U(t)|\text{ini}\rangle$ , i.e. the state obtained by evolving  $|\text{ini}\rangle$  to some time  $t$  and then back to  $t = 0$  again. If we Trotter-decompose the time evolution operator  $U(-t)$  into odd and even bonds in the reverse order of the decomposition of  $U(t)$ , the identity  $U(-t) = U(t)^{-1}$  holds without any Trotter error, and the forth-back deviation has the appealing property to capture the truncation error only.

As the DMRG setup used in this particular calculation did not allow easy access to the fidelity  $|\langle \text{ini} | fb(t) \rangle|$  (a calculation which is not a problem in principle, see [33]), the forth-back deviation was defined to be the  $L_2$  measure for the difference of the magnetization profiles of  $|\text{ini}\rangle$  and  $|fb(t)\rangle$ ,

$$FB(t) = \left( \sum_n (\langle \text{ini} | S_n^z | \text{ini} \rangle - \langle fb(t) | S_n^z | fb(t) \rangle)^2 \right)^{1/2}. \quad (33)$$

In order to control Trotter and truncation error, two DMRG control parameters are available, the number of DMRG states  $M$  and the Trotter time step  $dt$ .

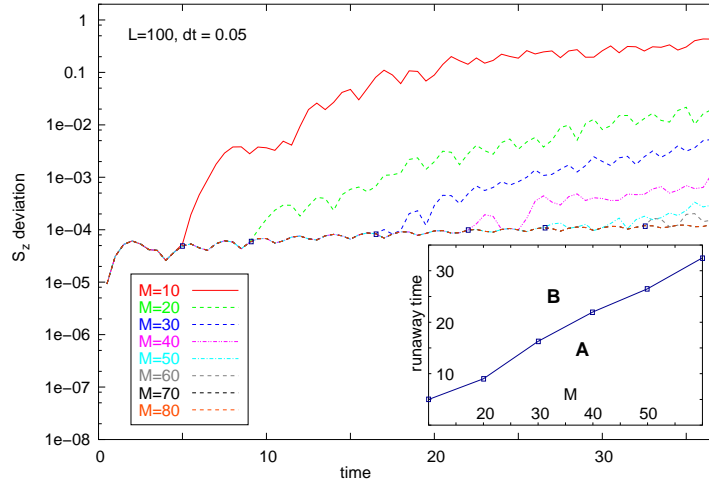


**Fig. 5:** Magnetization deviation  $\text{err}(t)$  as a function of time for different numbers  $M$  of DMRG states. The Trotter time interval is fixed at  $dt = 0.05$ . Again, two regimes can be distinguished: For early times, for which the Trotter error dominates, the error is slowly growing (essentially linearly) and independent of  $M$  (regime A); for later times, the error is entirely given by the truncation error, which is  $M$ -dependent and growing fast (almost exponential up to some saturation; regime B). The transition between the two regimes occurs at a well-defined “runaway time”  $t_R$  (small squares). The inset shows a monotonic, roughly linear dependence of  $t_R$  on  $M$ . From [34].

The dependence on  $dt$  is twofold: on the one hand, decreasing  $dt$  reduces the Trotter error by some power of  $dt^n$  exactly as in QMC; on the other hand, the number of truncations increases, such that the truncation error is enhanced. It is therefore not a good strategy to choose  $dt$  as small as possible. The truncation error can however be decreased by increasing  $M$ .

Consider the dependence of the magnetization deviation  $\text{err}(t)$  on the number  $M$  of DMRG states. In Fig. 5,  $\text{err}(t)$  is plotted for a fixed Trotter time step  $dt = 0.05$  and different values of  $M$ . One sees that a  $M$ -dependent “runaway time”  $t_R$  separates two regimes: for  $t < t_R$  (regime A), the deviation grows essentially linearly in time and is independent of  $M$ , for  $t > t_R$  (regime B), it suddenly starts to grow more rapidly than any power-law as expected of the truncation error. In the inset of Fig. 5,  $t_R$  is seen to increase roughly linearly with growing  $M$ . As  $M \rightarrow \infty$  corresponds to the complete absence of the truncation error, the  $M$ -independent bottom curve of Fig. 5 is a measure for the deviation due to the Trotter error alone and the runaway time can be read off very precisely as the moment in time when the truncation error starts to dominate.

That the crossover from a dominating Trotter error at short times and a dominating truncation error at long times is so sharp may seem surprising at first, but can be explained easily by observing that the Trotter error grows only linearly in time, but the accumulated truncation error grows almost exponentially in time.

To see that nothing special is happening at  $t_R$ , consider also Fig. 6, where the Trotter-error free  $FB(t)$  is plotted as a function of  $M$ , for  $t = 30$  and  $t = 50$ . An approximately exponential increase of the accuracy of the method with growing  $M$  is observed for a fixed time. Our numerical results that indicate a roughly linear time-dependence of  $t_R$  on  $M$  (inset of Fig. 5) are the consequence of some balancing of very fast growth of precision with  $M$  and decay of precision with  $t$ .

The runaway time thus indicates an imminent breakdown of the method and is a good, albeit



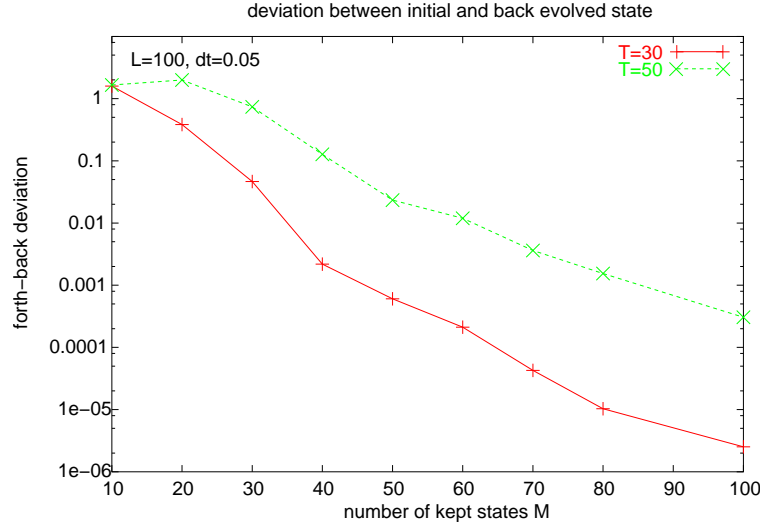


**Fig. 6:** The forth-back error  $FB(t)$  for  $t = 50$  and  $t = 30$ , as function of  $M$ . Here,  $L = 100$ ,  $dt = 0.05$ . From [34].

very conservative measure of available simulation times. We expect the above error analysis for the adaptive t-DMRG to be generic for other models. The truncation error will remain also in approaches that dispose of the Trotter error; maximally reachable simulation times should therefore be roughly the similar. Even if for high precision calculation the Trotter error may dominate for a long time, in the long run it is always the truncation error that causes the breakdown of the method at some point in time.

## 7 Spin-charge separation in ultracold atoms

Following the seminal work of Haldane [36], it has been understood that the low-energy behaviour of 1D quantum liquids is universally described by the Luttinger liquid (LL) picture [37, 38]. A remarkable prediction is spin-charge separation for Fermions: at low energy the excitations of charge and spin completely decouple and propagate with different velocities. The first unequivocal observation was obtained in experiments on the tunneling between two quantum wires [39]. A drawback of condensed-matter setups such as this is that the microscopic interactions strongly influence spin-charge separation, but are neither tunable nor known to some precision. Here, as in other condensed matter problems, the fact that in ultracold gases in optical lattices strong correlations can be studied with unprecedented control and tunability of the parameters might turn out to be very helpful. In fact, an 'atomic quantum wire' configuration in an array of thousands of parallel atom waveguides was realized in ultracold Fermi gases by the application of a strong two dimensional optical lattice [40]. Previous proposals to use cold atoms for studying spin-charge separation [41, 42] were limited by necessary analytical approximations, which do not hold for the strong and localized perturbations that would have to be created experimentally in current, relatively small systems. For a quantitative description of spin-charge separation one needs a microscopic description, which here is given almost perfectly by the Hubbard model. It is an essential new feature of cold atoms in optical lattices that parameters can be changed dynamically and the resulting time evolution can be studied. This gives direct access to the real-time dynamics of strongly correlated systems, an ideal testbed for

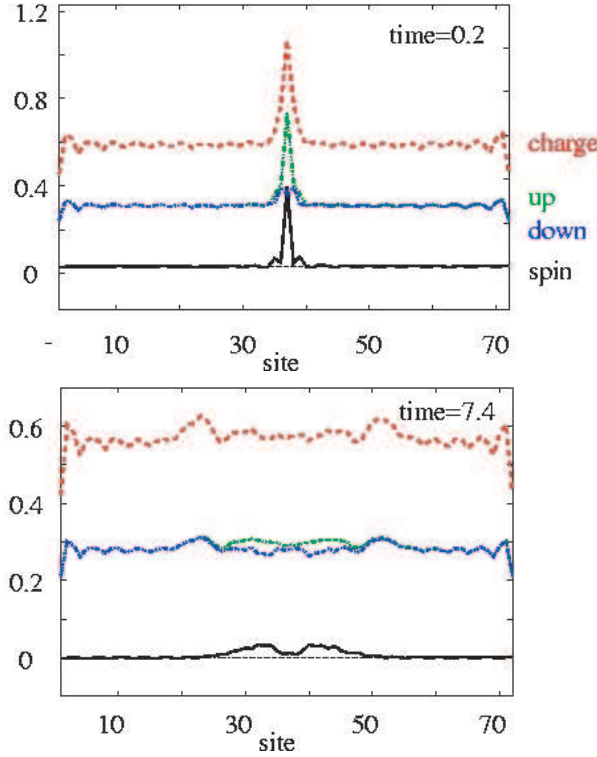


**Fig. 7:** A snapshot of the time-evolution of the charge and spin densities of a single particle excitation created at time  $t = 0$  at site  $j = 37$  is shown at  $t = 0.2$  and  $t = 7.4$ . Adapted from [32].

real-time DMRG: numerical results of the real-time dynamics of a 1D Hubbard model of up to 128 sites can be obtained easily [32].

We start from the standard Hubbard model

$$\begin{aligned}
 H = & -J \sum_{j,\sigma} \left( c_{j+1,\sigma}^\dagger c_{j,\sigma} + h.c. \right) + U \sum_j n_{j,\uparrow} n_{j,\downarrow} \\
 & + \sum_{j,\sigma} \varepsilon_{j,\sigma} \hat{n}_{j,\sigma}
 \end{aligned} \tag{34}$$

for Fermions in 1D, where we call the hopping matrix element  $J$ , to avoid confusion with time  $t$ . Setting  $J = 1$  and  $\hbar = 1$  time is measured in units of  $\hbar/J = 1$ . Special for the cold atom setup is a spin-dependent local on-site energy  $\varepsilon_{j,\sigma}$ , describing both a possible smooth harmonic confinement potential and time-dependent local potentials which allow to perturb the system. One introduces a 'charge' density  $n_c = n_\uparrow + n_\downarrow$  and a 'spin' density  $n_s = n_\uparrow - n_\downarrow$ ; in a realization with cold gases, where the spin degrees of freedom are represented by two different hyperfine levels, and 'charge' density is particle density. The ratio  $u = U/J$  can easily be changed experimentally by varying the depth of the optical lattice.

Experimentally, the density perturbations may be generated by a blue- or red-detuned laser beam tightly focused perpendicular to an array of atomic wires, which generates locally repulsive or attractive potentials for the atoms in the wires. In practice, the perturbations due to an external laser field are quite strong, typically of the order of the recoil energy  $E_r$  and thus clearly require a nonperturbative treatment.

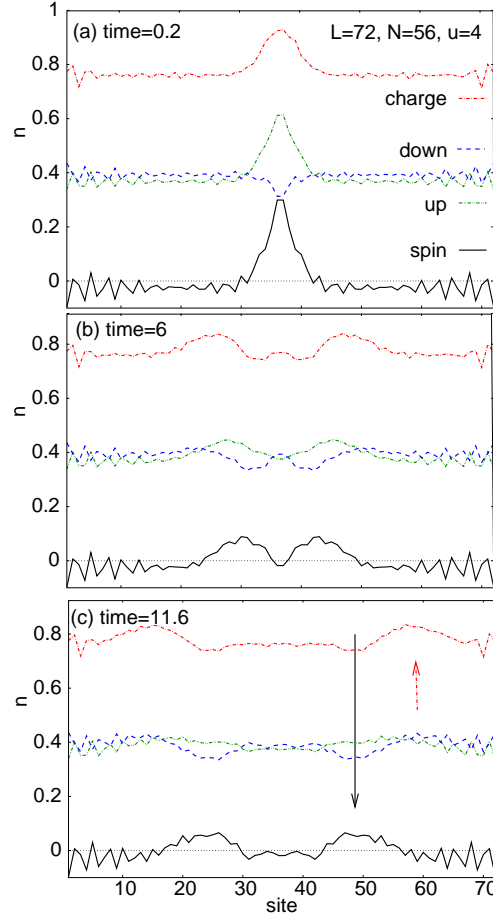


**Fig. 8:** Snapshots of the evolution of the density distribution are shown at different times. At  $t = 0$ , a wave packet is present in the center of the system in both the spin and the charge density. Each of these splits up into two packets which move with the same velocity in opposite directions. The velocity of the charge wave and the spin wave are different.  $u = U/J = 4$ , background density is  $n_0 = 0.78$ . Cf. [32].

In all following calculations system length was up to  $L = 128$  sites: several hundred DMRG states were kept. DMRG error analysis reveals that all density distributions shown are exact for all practical purposes, with controlled errors of less than  $O(10^{-3})$ .

In order to study the behaviour of a single particle excitation, the time evolution of the system with one additional particle with spin up added at time  $t = 0$  on site  $j$  to the ground state, was calculated numerically. In Fig. 7 a snapshot of the resulting evolution of the densities is shown for time  $t = 7.4$ . Remarkably, even after a such a short time separate wave packets in spin and charge can be seen.

In ultracold atom experiments, adding a single particle is not possible. Rather, spin-specific density perturbations can be created as discussed above. We therefore start with a homogeneous system which is perturbed by a potential  $\varepsilon_{j,\uparrow}$  localized at the chain center which couples only to the  $\uparrow$ -Fermions, i.e.

$$\varepsilon_{j,\uparrow}(t) \propto \exp \{ -[j - (L - 1)/2]^2/8 \} \theta(-t) \quad (35)$$

The potential is assumed to have been switched on slowly enough for equilibration, and is then switched off suddenly at time  $t = 0$ . In Fig. 8 (a) the density distribution of the state at an early

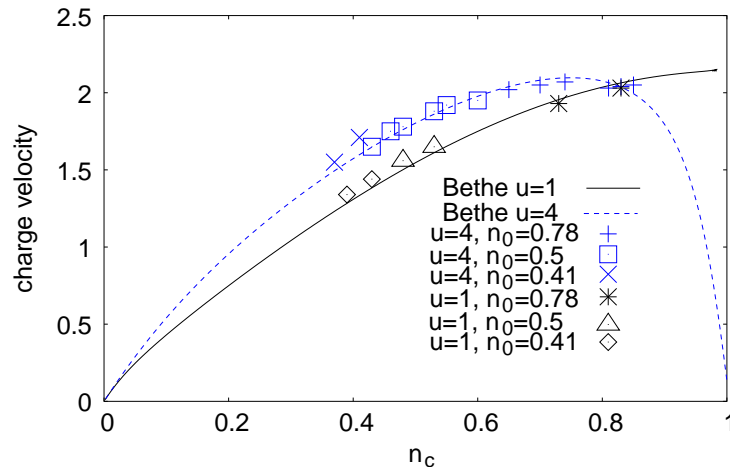


**Fig. 9:** Exact results for the charge velocity obtained by the Bethe ansatz are (lines) compared to the numerical results of the adaptive  $t$ -DMRG. The numerical results correspond to different heights of the perturbations at various charge background densities  $n_0$ .  $n_c$  is the charge density at the maximum/minimum of the charge density perturbation. The uncertainties are of the order of the size of the symbols and stem mainly from the determination of the velocity. From [32].

time is shown as obtained by DMRG. The external potential (35) generates a dominant perturbation in the  $\uparrow$ -Fermion distribution by direct coupling and, indirectly, a smaller perturbation in the  $\downarrow$ -density due to the repulsive interaction between the different spin species. The wave packets in  $\uparrow$  and  $\downarrow$ -density hence perform a complicated time evolution (Fig. 8). In contrast, the perturbations in the spin and charge density split into two wave packets each moving outwards. Their respective velocities are found to be different as indicated by the arrows in Fig. 8 (b), separating spin and charge.

In the limit of an infinitesimal perturbation much broader than the average interparticle spacing, both spin and charge velocities are known analytically from the Bethe ansatz [43]. To compare our numerical findings to the exact charge velocity, we create pure charge density perturbations, by applying the potential of Eq. (35) to both species, i.e.  $\varepsilon_{j,\uparrow} = \varepsilon_{j,\downarrow}$ , and calculate their time-evolution after switching off the potential. The charge velocity is determined from the propagation of the maximum (minimum) of the charge density perturbation for bright (amplitude  $\eta_c > 0$ ) and grey ( $\eta_c < 0$ ) perturbations, respectively. In Fig. 9 the charge velocities for various background densities  $n_0$  and perturbation amplitudes  $\eta_c$  are shown. We find good agreement, if we plot the charge velocity versus the charge density at the maximum (minimum), i.e.  $n_c = n_0 + \eta_c$ . The velocity of the maximum (minimum) of the wave packet is therefore determined by the value of the charge density at the maximum (minimum), not the background density.

This stays true even for strong perturbations  $\eta_c \approx \pm 0.1$  which corresponds to 20% of the charge density. The charge velocity is thus robust against separate changes of the background density  $n_0$  and the height of the perturbation  $\eta_c$ .

The previous results indicate that adaptive time-dependent DMRG is a highly performing method, able to answer complicated questions of dynamics in strongly correlated systems. To actually connect to experiments in the context of ultracold atoms, one has to take into account also the harmonic trapping potential, which may lead to a coexistence between a liquid (charge conduct-

ing) phase at the edges and a Mott-insulating phase in the center of the trap. Also, experiments can only measure quantities averaged over  $\sim 10$  lattice sites. These questions can be addressed in detail by DMRG; as they are not pertinent here, I refer to the literature [32].

## 8 Finite temperature

After the previous discussion on the difficulties of simulating the time-evolution of pure states in subsets of large Hilbert spaces it may seem that the time-evolution of mixed states (density matrices) is completely out of reach. It is however easy to see that a thermal density matrix  $\hat{\rho}_\beta \equiv \exp[-\beta\hat{H}]$  can be constructed as a pure state in an enlarged Hilbert space and that Hamiltonian dynamics of the density matrix can be calculated considering just this pure state (dissipative dynamics being more complicated). In the DMRG context, this has first been pointed out by Verstraete, Garcia-Rípol and Cirac [44] and Zwolak and Vidal [45], using essentially information-theoretical language; it has also been used previously in pure statistical physics language in e.g. high-temperature series expansions [46].

To this end, consider the completely mixed state  $\hat{\rho}_0 \equiv 1$ . Let us assume that the dimension of the local physical state space  $\{|\sigma_i\rangle\}$  of a physical site is  $N$ . Introduce now a local auxiliary state space  $\{|\tau_i\rangle\}$  of the same dimension  $N$  on an auxiliary site. The local physical site is thus replaced by a rung of two sites, and a one-dimensional chain by a two-leg ladder of physical and auxiliary sites on top and bottom rungs. Prepare now each rung  $i$  in the Bell state

$$|\psi_0^i\rangle = \frac{1}{\sqrt{N}} \left[ \sum_{\sigma_i=\tau_i}^N |\sigma_i\tau_i\rangle \right]. \quad (36)$$

Other choices of  $|\psi_0^i\rangle$  are equally feasible, as long as they maintain in their product states maximal entanglement between physical states  $|\sigma_i\rangle$  and auxiliary states  $|\tau_i\rangle$ . Evaluating now the expectation value of some local operator  $\hat{O}_\sigma^i$  acting on the physical state space with respect to  $|\psi_0^i\rangle$ , one finds

$$\langle\psi_0^i|\hat{O}_\sigma^i|\psi_0^i\rangle = \sum_{\sigma_i=\tau_i} \sum_{\sigma'_i=\tau'_i} \frac{1}{N} \left[ \langle\sigma_i\tau_i|\hat{O}_\sigma^i \otimes 1_\tau^i|\sigma'_i\tau'_i\rangle \right].$$

The double sum collapses to

$$\langle\psi_0^i|\hat{O}_\sigma^i|\psi_0^i\rangle = \frac{1}{N} \sum_{\sigma_i=1}^n \langle\sigma_i|\hat{O}_\sigma^i|\sigma_i\rangle,$$

and we see that the expectation value of  $\hat{O}_\sigma^i$  with respect to the pure state  $|\psi_0^i\rangle$  living on the product of physical and auxiliary space is identical to the expectation value of  $\hat{O}_\sigma^i$  with respect to the completely mixed local physical state, or

$$\langle\hat{O}_\sigma^i\rangle = \text{Tr}_\sigma \hat{\rho}_0^i \hat{O}_\sigma^i \quad (37)$$

where

$$\hat{\rho}_0^i = \text{Tr}_\tau |\psi_0^i\rangle\langle\psi_0^i|. \quad (38)$$

This generalizes from rung to ladder using the density operator

$$\hat{\rho}_0 = \text{Tr}_\tau |\psi_0\rangle\langle\psi_0|, \quad (39)$$

where

$$|\psi_0\rangle = \prod_{i=1}^L |\psi_0^i\rangle \quad (40)$$

is the product of all local Bell states, and the conversion from fictitious pure state to physical mixed state is achieved by tracing out all auxiliary degrees of freedom.

At finite temperatures  $\beta > 0$  one uses

$$\hat{\rho}_\beta = e^{-\beta\hat{H}/2} \cdot 1 \cdot e^{-\beta\hat{H}/2} = \text{Tr}_\tau e^{-\beta\hat{H}/2} |\psi_0\rangle \langle \psi_0| e^{-\beta\hat{H}/2},$$

where we have used Eq. (39) and the observation that the trace can be pulled out as it acts on the auxiliary space and  $e^{-\beta\hat{H}/2}$  on the physical space. Hence,

$$\hat{\rho}_\beta = \text{Tr}_\tau |\psi_\beta\rangle \langle \psi_\beta|, \quad (41)$$

where  $|\psi_\beta\rangle = e^{-\beta\hat{H}/2} |\psi_0\rangle$ . Similarly, this finite-temperature density matrix can now be evolved in time by considering  $|\psi_\beta(t)\rangle = e^{-i\hat{H}t} |\psi_\beta(0)\rangle$  and  $\hat{\rho}_\beta(t) = \text{Tr}_\tau |\psi_\beta(t)\rangle \langle \psi_\beta(t)|$ . The calculation of the finite-temperature time-dependent properties of, say, a Hubbard chain, therefore corresponds to the imaginary-time and real-time evolution of a Hubbard ladder prepared to be in a product of special rung states. Time evolutions generated by Hamiltonians act on the physical leg of the ladder only. As for the evaluation of expectation values both local and auxiliary degrees of freedom are traced on the same footing, the distinction can be completely dropped but for the time-evolution itself. Code-reusage is thus almost trivial. Note also that the initial infinite-temperature pure state needs only  $M = 1$  block states to be described exactly in DMRG as it is a product state of single local states. Imaginary-time evolution (lowering the temperature) will introduce entanglement such that to maintain some desired DMRG precision  $M$  will have to be increased.

## 9 Conclusion

Already the most powerful method for 1D statics and thermodynamics, DMRG is currently undergoing a second revolution. Beyond time-evolution in 1D, which was the main focus of this lecture, I expect DMRG to also have large impact on 2D quantum systems in the near future, as well as on the physics of quantum impurities [47]. The latter might have important implications for techniques such as the dynamical mean-field theory [48] for the modelling of realistic solids, which is limited by the need for highly efficient and precise quantum impurity solvers.

## References

- [1] S.R. White: Phys. Rev. Lett. **69**, 2863 (1992)
- [2] S.R. White: Phys. Rev. B **48**, 10345 (1993)
- [3] U. Schollwöck: Rev. Mod. Phys. **77**, 259 (2005)
- [4] M. Greiner, O. Mandel, T. Esslinger, T. W. Hänsch and I. Bloch: Nature (London) **415**, 39 (2002)
- [5] M. Köhl, H. Moritz, T. Stöferle, K. Günter and T. Esslinger: Phys. Rev. Lett. **94**, 080403 (2005)
- [6] G. Vidal: Phys. Rev. Lett. **93**, 040502 (2004)
- [7] A. J. Daley, C. Kollath, U. Schollwöck and G. Vidal: J. Stat. Mech.: Theor. Exp. (2004) P04005
- [8] S. R. White and A. Feiguin: Phys. Rev. Lett. **93**, 076401 (2004)
- [9] A. Feiguin and S. R. White: Phys. Rev. B **72**, 020404 (2005)
- [10] M. Fannes, B. Nachtergaele and R. F. Werner: Europhys. Lett. **10**, 633 (1989)
- [11] M. Fannes, B. Nachtergaele and R. F. Werner: Comm. Math. Phys. **144**, 3 (1992)
- [12] A. Klümper and A. Schadschneider and J. Zittartz: Europhys. Lett. **24**, 293 (1993)
- [13] S. Östlund and S. Rommer: Phys. Rev. Lett. **75**, 3537 (1995)
- [14] J. Dukelsky, M.A. Martin-Delgado, T. Nishino and G. Sierra: Europhys. Lett. **43**, 457 (1998)
- [15] H. Takasaki, T. Hikiyara and T. Nishino: J. Phys. Soc. Jpn. **68**, 1537 (1999)
- [16] F. Verstraete, D. Porras and J. I. Cirac: Phys. Rev. Lett. **93**, 227205 (2004)
- [17] S. R. White: Phys. Rev. Lett. **77**, 3633 (1996)
- [18] S. R. White: cond-mat/0508709
- [19] J. I. Latorre, E. Rico and G. Vidal: Quantum Inf. Comput. **4**, 48 (2004)
- [20] J. Gaite, quant-ph/0301120
- [21] C. Callan and F. Wilczek, Phys. Lett. **333**, 55 (1994)
- [22] J. Gaite, Mod. Phys. Lett. A **16**, 1109 (2001)
- [23] F. Verstraete and J. I. Cirac, cond-mat/0407066
- [24] T. Kühner and S.R. White, Phys. Rev. B **60**, 335 (1999)
- [25] E. Jeckelmann, Phys. Rev. B **66**, 045114 (2002)

- [26] M. Cazalilla and B. Marston: Phys. Rev. Lett. **88**, 256403 (2002)
- [27] H. G. Luo, T. Xiang and X. Q. Wang: Phys. Rev. Lett. **91**, 049701 (2003)
- [28] P. Schmitteckert: Phys. Rev. B **70**, 121302 (2004)
- [29] G. Vidal: Phys. Rev. Lett. **91**, 147902 (2003)
- [30] M. Suzuki: Prog. Theor. Phys. **56**, 1454 (1976)
- [31] C. Kollath, U. Schollwöck, J. von Delft and W. Zwerger: Phys. Rev. A **71**, 053606 (2005)
- [32] C. Kollath, U. Schollwöck and W. Zwerger: Phys. Rev. Lett. **95**, 176401 (2005)
- [33] S. Trebst, U. Schollwöck, M. Troyer and P. Zoller: cond-mat/0506809
- [34] D. Gobert, C. Kollath, U. Schollwöck and G. Schütz: Phys. Rev. E **71**, 036102 (2005)
- [35] T. Antal, Z. Racz, A. Rakos, G. Schütz: Phys. Rev. E **59**, 4912 (1999)
- [36] F. D. M. Haldane, J. Phys. C: Solid State Phys. **14**, 2585 (1981); Phys. Rev. Lett. **47**, 1840 (1981).
- [37] J. Voit, Rep. Prog. Phys. **58**, 977 (1995).
- [38] T. Giamarchi, *Quantum physics in one dimension*, Oxford, 2004 (Oxford University press).
- [39] O. M. Auslaender *et al.*: Science **308**, 88 (2005).
- [40] H. Moritz, Th. Stöferle, K. Günter, M. Köhl and T. Esslinger: Phys. Rev. Lett. **94**, 210401 (2005).
- [41] A. Recati, P.O. Fedichev, W. Zwerger and P. Zoller: Phys. Rev. Lett. **90**, 020401 (2003).
- [42] L. Kecke, H. Grabert, W. Häusler, Phys. Rev. Lett. **94**, 176802 (2005).
- [43] E.H. Lieb and F.Y. Wu, Phys. Rev. Lett. **20**, 1445 (1968). H. Shiba, Phys. Rev. B **6**, 930 (1972). C. F. Coll, Phys. Rev. B **9**, 2150 (1974). H.J. Schulz, Phys. Rev. Lett. **64**, 2831 (1990).
- [44] F. Verstraete, J. J. Garcia-Rípoll and J. I. Cirac: Phys. Rev. Lett. **93**, 207204 (2004)
- [45] M. Zwolak and G. Vidal: Phys. Rev. Lett. **93**, 207205 (2004)
- [46] A. Bühler, N. Elstner and G. S. Uhrig: Eur. Phys. J. B **16**, 475 (2000)
- [47] F. Verstraete, A. Weichselbaum, U. Schollwöck, I. Cirac and J. von Delft: cond-mat/0504305
- [48] A. Georges, G. Kotliar, W. Krauth and M. J. Rozenberg: Rev. Mod. Phys. **68**, 13 (1996)